Fuel 406 (2026) 136698

Contents lists available at ScienceDirect

Fuel

journal homepage: www.elsevier.com/locate/fuel

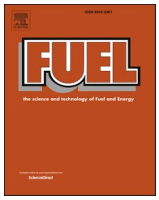

Full Length Article

Intensifying synthetic natural gas production by functionalization of a NiFe/γ-Al_2O_3 catalyst with alkaline and alkaline-earth materials

V.D. Mercader, P. Sanz-Monreal, P. Durán, P. Aragüés-Aldea, E. Francés, J. Herguido, J.A. Peña *

Catalysis and Reactor Engineering Group (CREG), Aragon Institute of Engineering Research (I3A), Universidad Zaragoza, 50.018 Zaragoza, Spain

ARTICLE INFO

Keywords:
Biogas upgrading
Carbon capture
CO_2 methanation
Dual function materials
Synthetic natural gas
Renewable hydrogen

ABSTRACT

This study demonstrates the influence of the functionalization method (Mechanical Mixture -MM- and Dual Function Materials -DFM-) of two CO_2 adsorbent species (Na and Ca) in a catalytic fixed-bed reactor for CO_2 methanation. The experiments consisted of cycles beginning with a CO_2 adsorption stage followed by a methanation stage (with H_2), interspersed with or without inert purge periods. The greatest enhancement in methane generation was observed in experiments with a mechanical mixture (MM) of NiFe/γ-Al_2O_3 catalyst and Na_2O/γ-Al_2O_3. The methane production capacity was tested over a temperature range comprised between 200 and 400 °C, with values over 380 μmol/g obtained under moderate conditions (350 °C and p_{CO2} = 0.12 bar) and selectivity to methane close to 100 %. Since the ultimate goal is the methanation of the CO_2 present in a biogas (without removing CH_4), the potential effect of the presence of methane during the CO_2 adsorption stages was also investigated. To achieve this task, a feed stream representative of a sweetened biogas coming from the anaerobic decomposition of municipal solid waste (MSW) (70 $\%^{V}$ CH_4 and 30 $\%^{V}$ CO_2) was used. The results showed no adverse effects along the successive cycles, paving the way to the use of these solids for biogas upgrading. On the other hand, the catalyst did not show a significant loss of activity after several hours of repetitive adsorption-methanation cycles.

1. Introduction

The transition to sustainable energy sources is a global priority, driven by the need to mitigate the effects of climate change and reduce greenhouse gas emissions, particularly carbon dioxide (CO_2), but also other agents such as short-chain hydrocarbons (e.g., CH_4) [1]. Fossil fuel-based energy systems remain a major contributor to global warming, forcing the adoption of cleaner and more sustainable technologies [2]. In recent years, progress has been made in the deployment of renewable energy technologies, especially solar photovoltaics and wind power [3]. However, their integration faces limitations, including intermittency, seasonal variability, and storage challenges, which hinder their capacity to fully meet global energy demands [4].

In parallel, advanced carbon management strategies have been explored to mitigate the environmental impacts of carbon emissions. Conventional methods like carbon capture and sequestration (CCS) have been implemented to trap CO_2 from point sources and store it underground. Yet, the CCS approach faces challenges, including high energy consumption, significant operational costs, and risks of CO_2 leakage from storage sites [5,6]. In this context, the integration of carbon capture and utilization (ICCU) has emerged as an alternative to transform CO_2 into valuable fuels and chemicals. ICCU technologies reduce the need for transportation and storage by enabling in-situ valorization of CO_2 [7,8]. A practical application of ICCU is embodied in the Power-to-Methane (PtM) process, wherein renewable energy is used to produce renewable hydrogen via water electrolysis. Subsequently, hydrogen reacts with captured CO_2 (Sabatier reaction, r.1 [9]) to generate biomethane – also known as synthetic natural gas (SNG) or renewable natural gas (RNG). Mechanistically, this reaction can be understood as proceeding through two consecutive steps: the reverse Water-Gas Shift (rWGS, r.2), followed by the reverse Steam Methane Reforming (rSMR, r.3). This process serves the dual purpose of storing renewable energy in chemical form (Power-to-X) and reducing greenhouse gas emissions [10,11]. The implementation of SNG within current natural gas infrastructure requires minimal adjustments, providing a viable solution for energy storage and distribution.

* Corresponding author.
E-mail address: jap@unizar.es (J.A. Peña).

https://doi.org/10.1016/j.fuel.2025.136698
Received 4 July 2025; Received in revised form 17 August 2025; Accepted 1 September 2025
Available online 19 September 2025

$$CO_2 + 4H_2 \rightleftharpoons CH_4 + 2H_2O \quad \Delta H_r^\circ = -165.1\ kJ{\cdot}mol^{-1} \tag{r.1}$$

$$CO_2 + H_2 \rightleftharpoons CO + H_2O \quad \Delta H_r^\circ = +41.2\ kJ{\cdot}mol^{-1} \tag{r.2}$$

$$CO_2 + 3H_2 \rightleftharpoons CH_4 + H_2O \quad \Delta H_r^\circ = -206.3\ kJ{\cdot}mol^{-1} \tag{r.3}$$

An alternative approach for integrating in-situ ICCU technologies into methanation processes has been proposed using dual-function materials (DFMs) [12–14]. DFMs often consist of an adsorbent and a metal active phase supported on a high surface area support [15]. As CO_2 storage components, various alkaline and alkaline-earth metal oxides and carbonates have been investigated, such as Na_2CO_3, K_2CO_3, and CaO [16]. These materials are capable of capturing CO_2 from diluted exhaust gases and converting it to methane in a single reactor. This concept implies a cyclic operation due to the sequential adsorption and hydrogenation steps. Depending on the strategy, the adsorbent can either be physically mixed with the catalyst or integrated within the same material structure (Fig. 1). Nevertheless, the implementation of multiple parallel reactors has been demonstrated to enable continuous methane production [17], allowing the omission of gas purification steps, which can result in reduced overall process costs. This configuration offers advantages, including optimizing heat inputs required for the hydrogenation stage [18], remaining mild conditions for the CO_2 capture improving the durability of the adsorbents. These materials must demonstrate the capacity to operate across a broad range of temperatures (200–500 °C) and in the presence of diverse gas mixtures, including CO_2, O_2, and H_2O, depending on the specific application and effluent characteristics [19,20]. In addition, recent studies of Zhou et al. [21,22] have shown the potential use of ICCU-M at temperatures exceeding 500 °C.

For CO_2 hydrogenation, a wide variety of single-metal and bimetallic formulations have been explored [23,24]. In conventional methanation, nickel-based catalysts are widely employed due to their favorable activity, availability, and low cost. Noble metals such as ruthenium offer high activity [25]; however, their scarcity and high cost limit their large-scale deployment [26]. Within the ICCU context, Ni-based catalysts have shown limitations, including reduced activity at low temperatures, susceptibility to deactivation via sintering at high temperatures, and oxidation to NiO in CO_2 − or O_2 − containing streams, rendering them inactive for methanation [27,28]. For instance, Bermejo et al. [29,30] reported that Ru/Ni-based DFMs supported on Na/Ca–Al_2O_3 exhibited distinct aging behaviors: while Ru enhanced long-term stability and sustained methanation rates, Ni-containing systems were more prone to deactivation. To overcome these issues, bimetallic catalysts (with Ni as a primary component) have been proposed to enhance activity, stability, and selectivity [31]. Bermejo et al. [32] observed that the presence of a promoter enhances both CO_2 storage and hydrogenation performance of the Ni/Na_2CO_3 catalyst at intermediate and high temperatures. Among the tested formulations, the Ru-promoted sample exhibited the highest CH_4 production [29]. Such combinations create synergistic effects that improve CO_2 conversion, modulate selectivity, and mitigate deactivation. Moreover, NiFe catalysts have demonstrated significantly higher CO_2 conversion and CH_4 selectivity compared to their single-metal counterparts [19]. The presence of iron facilitates CO_2 dissociation, avoiding coke formation and improving the reducibility of nickel [33]. Iron also contributes to cost reduction by partially substituting Ni with a cheaper metal.

Recent studies on DFMs have identified critical challenges related to the interaction between CO_2 adsorption and methanation functionalities. DFMs are often limited by the intrinsic competition between adsorption and catalytic sites [34]. Strong CO_2 binding on the adsorbent phase can reduce the accessibility of adjacent active metal sites, leading to incomplete hydrogenation and increased CO selectivity. This behavior underscores the importance of optimizing both spatial and chemical interactions between functionalities during DFM design [35]. Recent works have proposed the mechanochemical synthesis of DFM to improve the interaction between the active species present in the ICCU-

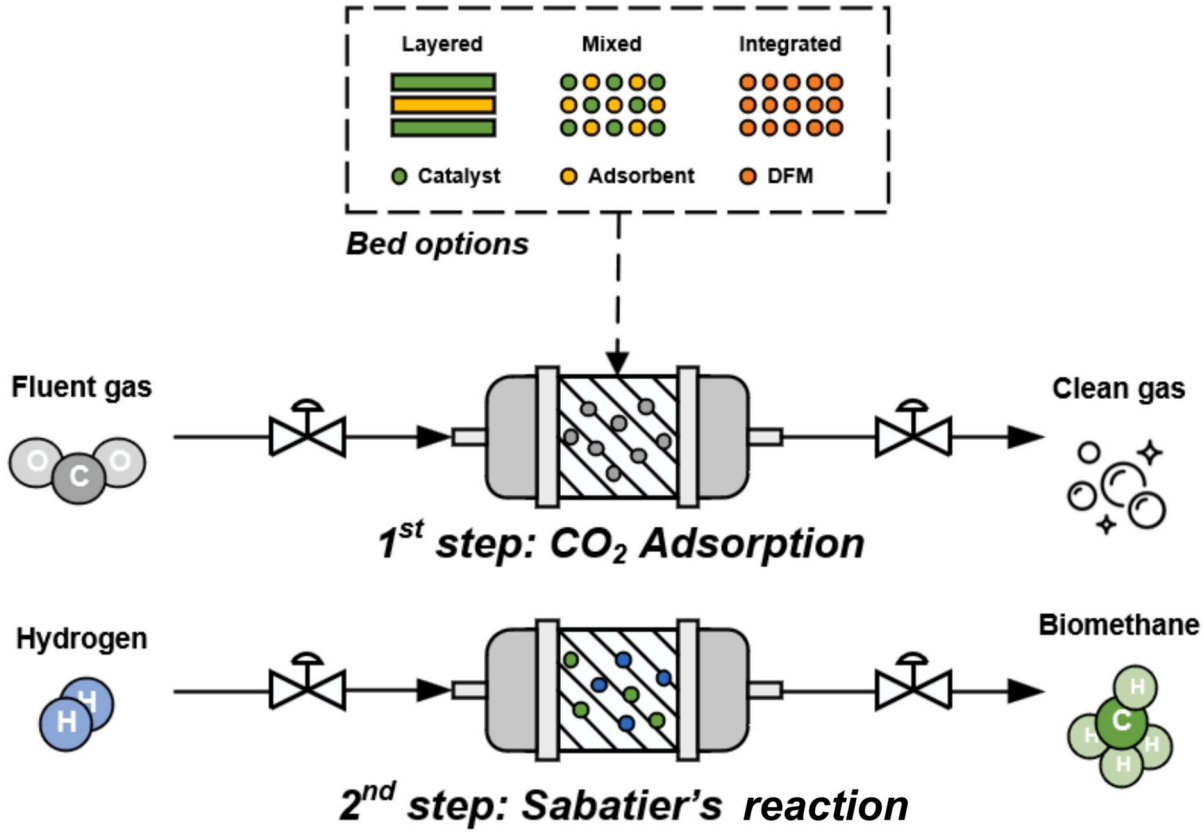

Fig. 1. Schematic of sequential CO_2 adsorption and hydrogenation via Sabatier reaction.

M process [36].

The advantages of separating adsorbents and catalysts have been investigated in recent years in other methanation technologies, such as the Sorption-Enhanced Sabatier Reaction (SESaR), also known as Sorption-Enhanced Methanation (SEM) [37]. This approach enhances methanation by in-situ water removal using hydrophilic adsorbents, such as zeolites [38]. Some authors, such as Wei L. et al. [39], have reported promising results using zeolites as support, leveraging their water adsorption capacity while integrating catalytic sites. Other studies [40,41], have demonstrated high methane yields and selectivity when separating the zeolite and the catalyst into two distinct solids, mechanically mixed within the methanation reactor.

DFMs have been widely referenced for cyclic methanation intensification [42,43]. However, their performance under conventional methanation conditions – where H_2 and CO_2 are co-fed into the reactor – has been less extensively studied. Some investigations have explored the effects of doping Ni catalysts with alkali and alkaline earth metals, revealing that the inclusion of small amounts of these elements (e.g., Ca) can positively influence selectivity and methane production [44]. For example, Mohammed et al. [45] studied the impact of adding 0.5 to 2 $\%^{wt}$ Ca to a Ni/Fumed-SiO_2 catalyst. Their findings indicated that 0.5 $\%^{wt}$ Ca was the optimal loading for conventional methanation, as higher Ca concentrations reduced the intensification effect compared to the unmodified catalyst. Since many DFMs reported in the literature contain around 10 $\%^{wt}$ alkali species [46–48,49], this study considers it relevant to evaluate both DFMs and mechanically mixed (MM) materials—originally designed for cyclic methanation—under conventional methanation conditions. Achieving a homogeneous distribution of both solids along the fixed bed is essential; in this study, this distribution is obtained through mechanical mixing. The combined material is referred to throughout this work as Mechanical Mixture (MM).

In this work, a novel strategy is proposed wherein CO_2 adsorption and methanation functions are separated into two distinct solids. The first solid contains the active species for methanation, specifically a bimetallic Ni:Fe catalyst in a 3:1 wt ratio supported on γ-Al_2O_3, based on previous research by this group [33] and corroborated by recent literature [50]. To evaluate this concept, two CO_2 adsorbents were synthesized using alkali or alkaline earth metals, each supported on γ-Al_2O_3. The resulting materials contained 10 $\%^{wt}$ Na or 10 $\%^{wt}$ Ca and were labeled "Na_2O" and "CaO," respectively. Prior work [30] has studied the effect of incorporating Na and Ca into Ni/γ-Al_2O_3 catalysts, showing enhanced methane production in CO_2 adsorption-hydrogenation systems. Additionally, other studies [51] have proposed K and Li as more stable alternatives to Na in Ru-based catalysts. However, in the present study, Ca and Na were selected due to their lower cost and wide availability.

The main objective of this work is to experimentally evaluate and quantify the performance of the Sabatier reaction (r.1) under CO_2 adsorption-hydrogenation cycles in a fixed-bed reactor. Specifically, the effects of the presence of a CO_2 adsorbent in the catalytic bed, reaction temperature, and the use of synthetic sweetened biogas as a CO_2 source are studied. Experiments are conducted using a mechanically mixed configuration that combines the NiFe-based catalyst with either Na_2O or CaO-based adsorbents. This strategy aims to bridge the gap between traditional DFMs and more flexible, modular process configurations suitable for industrial scale methanation applications.

2. Experimental

2.1. Catalyst preparation and characterization

All catalysts were synthesized by the incipient wetness impregnation method on commercial γ-Al_2O_3 (200.6 ± 0.4 m^2/g; *Puralox*, *SASOL*). The precursors used for catalyst synthesis were: $Ni(NO_3)_2{\cdot}6H_2O$ (98.6 %; *Sigma-Aldrich*), $Fe(NO_3)_3{\cdot}9H_2O$ (>98 %; *Sigma-Aldrich*), and $Ca(NO_3)_2{\cdot}4H_2O$ (99.98 %; *Alfa Aesar*) and Na_2CO_3 (99.5 %; *Panreac*) for adsorbents species incorporation.

DFM synthesis consisted of two consecutive impregnation steps. The first step introduced the CO_2 adsorbent species onto the γ-Al_2O_3 support, followed by drying and calcination. The second impregnation incorporated the methanation catalytic species (Ni or NiFe).

Since γ-Al_2O_3 has been the support for all the solids mentioned across this work, for the sake of simplicity, all mentions to the catalyst or the CO_2 adsorption materials will omit the express mention to the support, alluding only to the active phase (Ni or NiFe for catalyst and Na_2O or CaO for CO_2 adsorption species).

To study the optimal method for functionalizing the solids with CO_2 adsorbent species, up to three catalysts (*Dual Function Materials*, DFMs) were synthetized. Two contained an active phase composition of 7.5:2.5 $\%^{wt}$ Ni:Fe, and one had 10 $\%^{wt}$ Ni. These were functionalized respectively with: a) 10 $\%^{wt}$ Ca (labeled "CaNiFe"), b) 10 $\%^{wt}$ Na ("NaNiFe"), and c) 10 $\%^{wt}$ Na corresponding to a reference catalyst from the literature ("NaNi") [32]. Additionally, two other catalysts were prepared as mechanical mixtures (MM) of the CO_2 adsorbent (10 $\%^{wt}$ CaO or 10 $\%^{wt}$ Na_2O) with the same active phases mentioned above (10 $\%^{wt}$ Ni or 7.5:2.5 $\%^{wt}$ Ni:Fe).

An overall of all the synthetized solids is presented in Table 1.

After impregnation, the catalyst was dried at 65 °C for 16 h and then at 90 °C for 8 h. Once dried, it was calcined at 500 °C for 9 h (β = 1 °C/min). Subsequently, it was crushed and sieved to obtain the appropriate particle size. Mechanical mixtures (MM) where prepared from the already synthesized solids on a separate manner, mixed on a beaker until homogeneous mix, and finally introduced carefully in the reactor.

Prior to any experiment, the catalyst was activated at 500 °C for 2 h with a flowrate of 150 mL (SATP)/min in an atmosphere composed of 50 $\%^{v}$ H_2, 45 $\%^{v}$ Ar and 5 $\%^{v}$ N_2. Pressure was always 1 bar.

A series of preliminary experiments were conducted in order to select the optimal reaction conditions and catalyst composition. Prior, diffusional limitations in the packed bed (external and internal) were checked to discard them. As consequence, a flowrate of 150 mL(SATP)/min was found to be sufficient to ensure kinetic regime control. Also, the particle size was adjusted to the range 100–200 μm with the same purpose.

Adsorption stages were performed feeding a flowrate of 150 mL (SATP)/min with 12 to 40 $\%^{v}$ of CO_2, 5 $\%^{v}$ N_2 (internal standard) plus Ar to balance. Hydrogenation stages with same flowrate but with 5 $\%^{v}$ of H_2 plus 90 $\%^{v}$ Ar and 5 $\%^{v}$ N_2 playing the same role.

The adsorption capacity of the solids bed in the presence of a CO_2 flow was determined by measuring its outlet concentration using a micro-gas chromatograph (Agilent 490), supported by a continuous IR

Table 1
Synthetized solids description.

Solids	Nominal composition ($\%^{wt}$)	Role
Ni	10Ni/γ-Al_2O_3	Catalyst
NiFe	7.5Ni-2.5Fe/γ-Al_2O_3	
Na_2O	10Na/γ-Al_2O_3	CO_2 adsorbent / promotor
CaO	10Ca/γ-Al_2O_3	
NaNi	10Na-10Ni/γ-Al_2O_3	Dual Function Material (DFM)
NaNiFe	10Na-7.5Ni-2.5Fe/γ-Al_2O_3	
CaNiFe	10Ca-7.5Ni-2.5Fe/γ-Al_2O_3	
Na_2O + Ni	10Na/γ-Al_2O_3 + 10Ni/γ-Al_2O_3	Mechanical Mixture (MM)
Na_2O + NiFe	10Na/γ-Al_2O_3 + 7.5Ni-2.5Fe/γ-Al_2O_3	
CaO + Ni	10Ca/γ-Al_2O_3 + 10Ni/γ-Al_2O_3	
CaO + NiFe	10Ca/γ-Al_2O_3 + 7.5Ni-2.5Fe/γ-Al_2O_3	

gas analyzer (Servomex Series 4000). The equilibrium adsorption capacity was corroborated by thermogravimetric analysis (TGA) under representative experimental temperatures and CO_2 partial pressures in the feed. TGA measurements were performed using a simultaneous thermal analyzer (STA 449 F1 Jupiter, *NETZSCH*).

The catalyst characterization was carried out through specific surface area quantification by nitrogen adsorption–desorption (BET) after degassing at 200 °C, elemental analysis by X-Ray fluorescence (XRF), dispersion of active sites by scanning electron microscopy with energy-dispersive X-Ray spectroscopy (SEM-EDX), crystallinity by X-Ray diffraction (XRD) (not shown), and temperature-programmed reduction (TPR) with a H_2/N_2 flow of 100 mL (SATP)/min and hydrogen partial pressure of 0.05 bar out of 1 bar of total pressure. In addition, the active sites dispersion was characterized by Field Emission Scanning Electron Microscope (FESEM) assisted with Energy-dispersive X-ray Spectroscopy (EDX) (*INSPECT* F50).

2.2. Stages in methanation experiments

2.2.1. Performance of DFM and MM in conventional methanation

To evaluate the potential use of DFM and MM in conventional methanation, the solids listed in Table 1 were tested in a fixed bed reactor under the conditions specified in Table 2. Comparing the performance of DFM under conventional methanation may help identify potential side effects associated with the incorporation of CO_2 adsorbent species into the catalyst formulation. Additionally, the results may shed light on the potentially negative impact of alkali species present in DFMs, as they may compete with Ni–Fe active sites for CO_2 adsorption, thereby affecting CO_2 conversion and methane yield.

For the reaction experiments with different catalysts, the mass of solids introduced into the bed (homogenously premixed) consistently comprised: 2 g of catalyst, 2 g of CO_2 adsorbent (Na_2O or CaO), and 6.5 g of γ-Al_2O_3.

2.2.2. Successive CO_2 adsorption – methanation cycles

Each cycle of the methanation experiment (Fig. 2 as example) included three stages: first, the reactor was fed with CO_2 diluted in inert gas (*adsorption stage*). After an optional *inertization* period (N_2), the inert gas was replaced by H_2 at the inlet (*hydrogenation stage*). Finally, only inert gases were introduced as an optional purge stage (N_2), beginning again with a second cycle with the same sequence. The concentration at the reactor outlet was quantified with a micro-gas chromatograph (*Agilent* 490) assisted by a continuous IR gas analyzer (*Servomex* series 4000).

Species analyzed at the exit of the reactor (Fig. 2) show, along the experiment in the CO_2 stage, a progressive increase of CO_2 present in the exhaust stream because of the saturation of the solid. This stage was followed by an inertization stage. Concentration and flowrates at different stages can be consulted in Table 2.

Table 2
Experimental conditions.

	Conventional Methanation	Adsorption + Methanation cycles
Catalyst mass	0.25 g	2 g
Adsorbent mass	–	2 g
Mass filler (γ–Al_2O_3 particles)	10.25 g	6.5 g
Volumetric flow	250 mL(SATP)/ min	150 mL(SATP)/ min
CO_2 concentration (adsorption step)	18 %^{v}	12/40 %^{v}
WHSV (SATP mL·g_{cat}^{-1}·h^{-1})	60,000	4500
CH_4:CO_2 molar ratio (biogas experiments)	–	7:3
H_2 concentration (methanation step)	72 %^{v}	5 %^{v}
N_2 concentration (int. standard)	5 %^{v}	5 %^{v}
Inert dilutant	Ar	Ar
Pressure	1 bar	1 bar
Temperature	200–400 °C	200–400 °C
Adsorption step length	–	30 min
Methanation step length	1 h	1 h 30 min

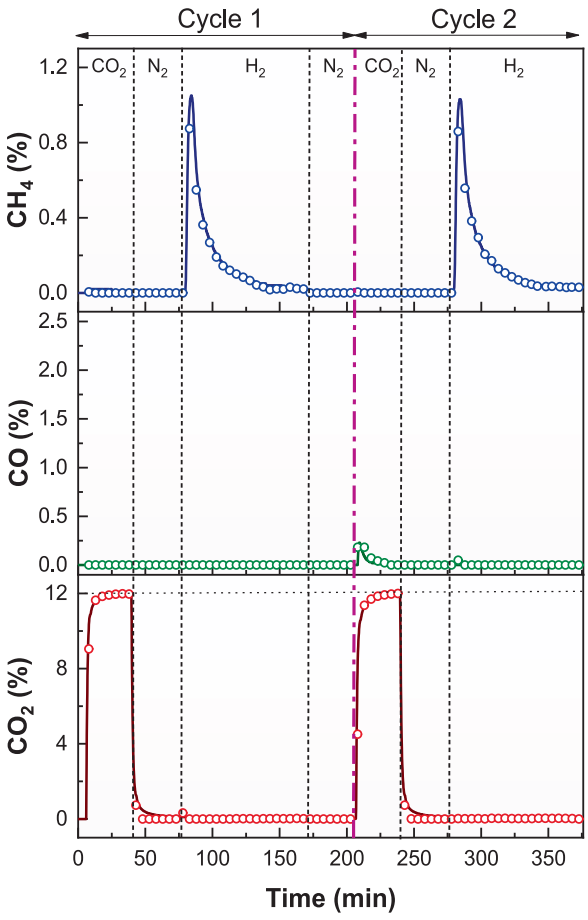

Fig. 2. Example of temporal evolution of gaseous species (reactants and products) at the exit of the reactor in a two-cycle experiment [adsorption of 12 %^{v} CO_2 + N_2 purge + hydrogenation (see Table 2)] with NiFe + Na_2O at 400 °C. Symbols: μGC readings; continuous lines: IR readings.

Respecting the hydrogenation stage, in which diluted H_2 was fed to the reactor, basically an intense production of methane was detected as consequence of the reactions (r.1) to (r.3). The same behavior was observed in the following cycle. Even in the CO_2 adsorption stage of 2nd cycle, a small amount of CO was detected, probably due to a partial smooth reoxidation of metallic species on the catalyst surface, or to an equilibrium between CO and CO_2 species related to alkaline or alkaline-earth carbonate formation. These patterns were quite similar for all the catalysts tested, being only the amount of CO_2 adsorbed and the amount of CH_4, each one in their respective stages, the most significant differences.

Omitting the purge step was proposed as a time intensification strategy for the CO_2 adsorption-methanation cycles. The purge stage with inert gas between the CO_2 adsorption and hydrogenation stages has been reported as a method to control CO production by removing weakly adsorbed CO_2 on the catalyst surface [28]. Nevertheless, the inert gas can partially displace the CO_2 adsorbed on the dual-function material (DFM) or mechanical mixture (MM). Additionally, in a more favorable sense, the use of inert gas between subsequent stages helps to remove adsorbed species still present on the solid after methanation (e.g., water), potentially reducing the competitive adsorption between water and CO_2.

In addition to the use of diluted CO_2 along the adsorption stage

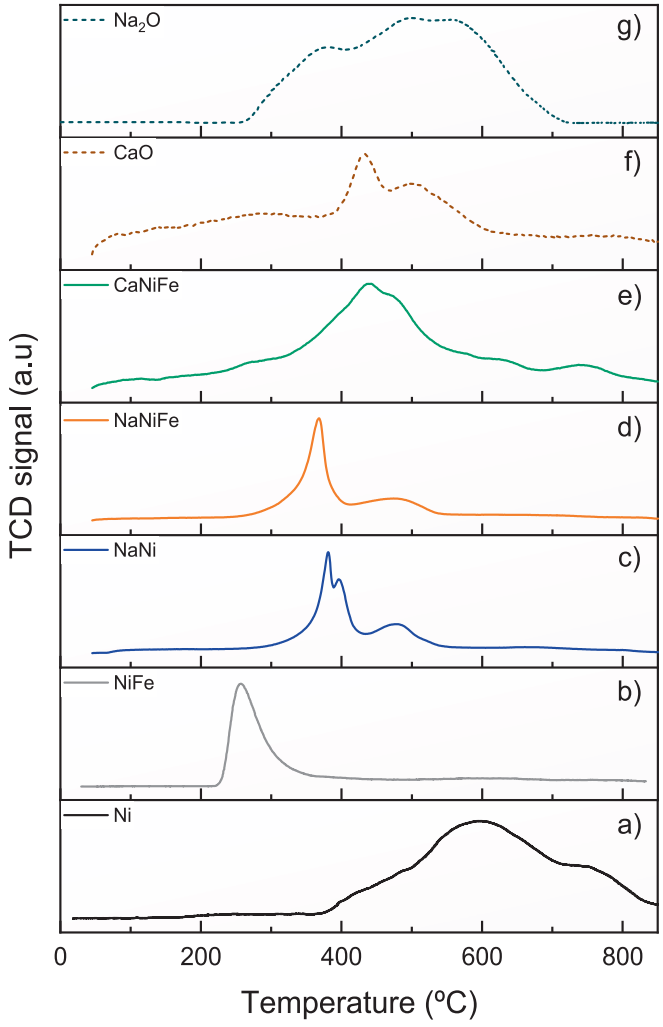

Fig. 3. TPR characterization for the DFM, CO_2 adsorbents and catalysts: a) Ni, b) NiFe, c) NaNi, d) NaNiFe, e) CaNiFe, f) CaO, g) Na_2O.

(Fig. 3), the incorporation of biogas as a source of the necessary CO_2 has also been studied. To do that, the stream of CO_2 has been replaced by a mixture of CH_4:CO_2 (7:3 molar ratio), representing a previously sweetened biogas. A blank experiment was conducted to quantify separately the CH_4 generated during the hydrogenation step from that one that could be unintentionally adsorbed in the bed coming from the biogas fed during the previous adsorption stage. This procedure allowed for the elimination of any potential contribution from unreacted biogas remaining in the system, ensuring an accurate evaluation of the methane thermocatalytically produced.

In this context, DFM or MM may have potential applications for biogas upgrading: the CO_2 present in the biogas stream would be captured by the DFM or MM which, in turn, would result in a highly concentrated CH_4 flow. During the subsequent hydrogenation step, the captured CO_2 would be converted into methane.

Temperature effect in the cyclic adsorption-methanation was studied under a temperature range comprised between 200 and 400 °C with the catalyst that provided the best methane production results.

2.2.3. Performance of the DFM and MM indicators

A series of indicators have been defined in order to account for the performance of the different solids described in previous chapters.

Intensification (I_{CH_4}) indicator (Eq. (1)) accounts for the μmol of CH_4 [$(\mu mol\, CH_4)_{DFM\ or\ MM}$] produced with the different combination of catalysts and adsorbents (DFM or MM), taking the amount of CH_4 produced by the NiFe/γ-Al_2O_3 without adsorbents [$(\mu mol\, CH_4)_{NiFe}$] as reference. The amount of μmol of CH_4 produced has been calculated from the area below the curve of CH_4 production, from the IR readings depicted in Fig. 2 (hydrogenation stage).

$$Intensification, I_{CH_4}[\text{adim}] = \frac{(\mu mol\, CH_4)_{DFM\ or\ MM}}{(\mu mol\, CH_4)_{NiFe}} \quad (1)$$

On the other hand, *Methane production* ($P^W_{CH_4}$) indicator (Eq. (2)), accounts for the μmoles of CH_4 [$(\mu mol\, CH_4)_{DFM\ or\ MM}$] produced with the different combination of catalysts and adsorbents (DFM or MM), respecting the mass of DFM or MM material present in the solid bed. As stated in Table 2, for the experimental series of this work, this value has always been 2 g.

$$Methane\ production, P^w_{CH_4}[\mu mol/g] = \frac{(\mu mol\, CH_4)_{DFM\ or\ MM}}{W(g)_{DFM\ or\ MM}} \quad (2)$$

Methanation yield (η_{CH_4}) indicator (Eq. (3)), accounts for the yield to CH_4 from CO_2, calculated as the ratio between the amount of μmol of CH_4 along the methanation stage per gram of DFM or MM (Fig. 2) and the μmol of CO_2 adsorbed in the equilibrium per gram of DFM or MM at the experimental conditions. These were corroborated by TGA analysis in the same conditions of CO_2 partial pressure and temperature as those employed in the reactor.

$$Methanation\ yield, \eta_{CH_4}[\text{adim}] = \frac{\mu mol\ CH_4\ produced}{\mu mol\ CO_2\ adsorbed\ in\ the\ solid} \quad (3)$$

3. Results and discussion

3.1. Catalyst characterization

BET results (Table 3) show a slight decrease in surface area after the impregnation of the active Ni-Fe phases onto the γ-Al_2O_3 matrix (220.6 ± 0.4 m^2/g). On the other hand, the inclusion of alkaline and alkaline-earth species causes a significant reduction in surface area and pore volume. Regarding elemental analysis, some reasonable deviations were found between nominal and quantified values, which are attributable to the catalyst synthesis process.

TPR results presented in Fig. 3 evidence the inclusion of Ni alone and co-impregnated Ni and Fe in the DFM synthesized, as well as new additional peaks from the alkali and/or alkaline carbonates species introduced. As can be observed in Fig. 3b, the impregnation of Ni and Fe from nitrates on a single step creates a bimetallic synergy with lower reduction temperature than Ni alone (Fig. 3a). Additionally, the inclusion of Na in the Al_2O_3 support improved the reducibility of Ni (Fig. 3c), decreasing the reduction temperature. This effect is even more noticeable for Ni-Fe based catalyst (Fig. 3d). Similar effects can be found in the sample including Ca as active sorbent species (Fig. 3e). Fig. 3f and Fig. 3g present the Ca and Na adsorbent solids (no catalytic species) used for mechanical mixture experiments. TPR results reveal the presence of carbonate precursors in the solids containing Ca and Na. This observation was expected, as the calcination temperature (500 °C) is lower than the thermal decomposition temperatures (over 900 K) of calcium carbonate and sodium carbonate [52]. The strong interaction between the alkali species and the carbonates can be disrupted in the presence of H_2, as evidenced in the TPR profiles.

The dispersion of active sites, as determined by FESEM-EDX analysis, is presented in Fig. 4. As observed, the active species were adequately dispersed across all samples. However, the surface morphology of the DFM was visibly affected by the incorporation of alkali species, exhibiting increased crust formation and surface irregularities. This alteration may be associated with the reduction in BET surface area observed in the solids functionalized with alkali content.

Table 3
Summary of characterization results of the solids tested. All of them used γ-Al_2O_3 as support completing balance (see Table 1).

Solid	BET area ($m^2 \cdot g^{-1}$)	BJH pore		XRF (%^{wt})				
		Radius (Å)	Volume ($cm^3 \cdot g^{-1}$)	Ni	Fe	Al	Ca	Na
γ-Al_2O_3	220.6 ± 0.4	36.37	0.43					
NiFe	167.4 ± 0.4	36.23	0.46	7.4 ± 0.1	2.1 ± 0.1	46.9 ± 0.3	–	–
CaNiFe	89.3 ± 0.4	36.03	0.29	9.6 ± 0.1	3.4 ± 0.1	35.1 ± 0.1	11.3 ± 0.1	
NaNiFe	113.6 ± 0.4	36.35	0.34	8.5 ± 0.1	2.6 ± 0.1	36.6 ± 0.1	–	11.44 ± 0.1
NaNi	82.2 ± 0.4	36.10	0.29	6.75 ± 0.1	–	42.3 ± 0.1	–	10.23 ± 0.1
CaO	98.3 ± 0.4	36.13	0.31		–	44.0 ± 0.1	11.7 ± 0.1	–
Na_2O	100.5 ± 0.4	36.19	0.35	–	–	42.5 ± 0.1	–	14.01 ± 0.3

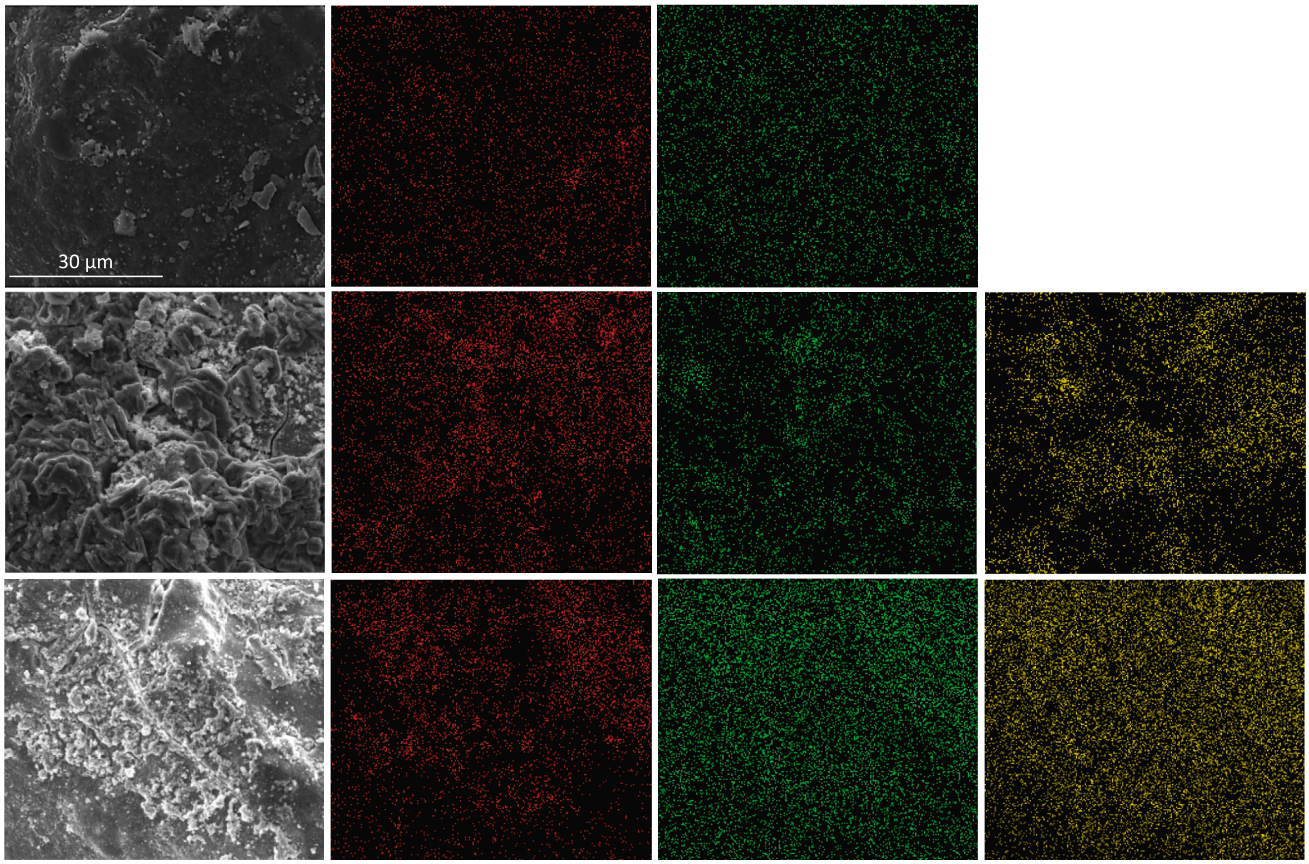

Fig. 4. FESEM-EDX images (left) for: 1st row) NiFe reference, 2nd row) NaNiFe, 3rd row) CaNiFe and EDX spectroscopy analysis showing the dispersion of iron (−red-), nickel (−green-) and sodium or calcium (−yellow-). (For interpretation of the references to colour in this figure legend, the reader is referred to the web version of this article.)

3.2. *Influence of the CO_2 adsorbent functionalization method*

3.2.1. *Conventional methanation*

Catalyst selection studies, methane production at different temperatures, and comparisons between CO_2 feed and biogas feed, were conducted under the conditions outlined in Table 2. Fig. 5 presents the effect of temperature in CO_2 conversion for different DFM and MM (Table 1) based on Ni and Ni-Fe species. The experiments were carried out under conventional stoichiometric methanation feeding H_2:CO_2 (4:1), with a reactants/inert volumetric ratio of 9:1 and a total flowrate of 250 mL (SATP)/min. For conventional methanation, the reactor described in Table 2 was filled with 0.25 g catalyst, DFM or equivalent active phase MM (0.25 g of catalyst +0.25 g of adsorbent), mixed with alumina until achieving a total bed weight of 10.5 g. As it can be observed in Fig. 5, Na and Ca presence in the DFM affected negatively the conversion of CO_2, in comparison with the reference *Ni* and *NiFe* catalysts. Also, the yield to methane (Fig. 6) decreased dramatically for all the DFM, due to their high selectivity to CO. On the other hand, MM showed similar results to the reference *NiFe* catalyst for the temperature range studied (250–400 °C) both, for conversion and for yield. In the case of *Ni*, MM exhibited a moderate loss in both CO_2 conversion and methane production.

3.2.2. *Cyclic CO_2 adsorption – Methanation cycles*

The study on methane production, influenced by the method of functionalizing the CO_2 adsorbent to the catalytic bed, is graphically summarized in Fig. 7. Two performance indicators: *Intensification* I_{CH_4}[adim] ratio (Eq. (1)), and *Methane production* $P^{w}_{CH_4}[\mu mol/g]$ ratio (Eq.

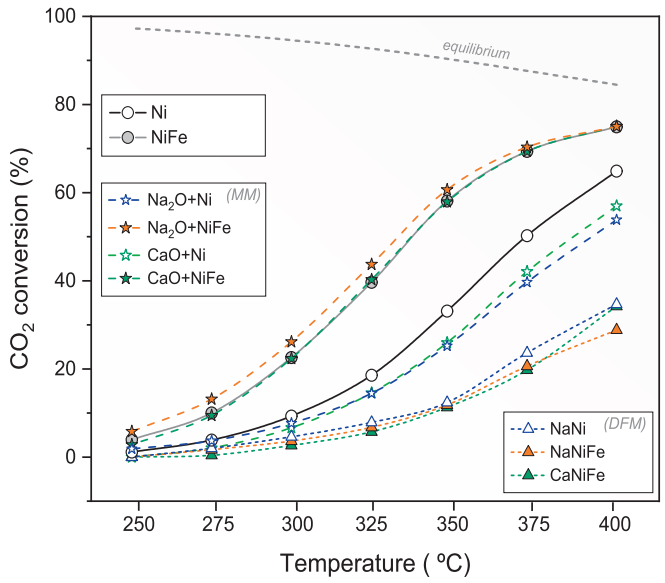

Fig. 5. Conventional methanation. CO_2 conversion as a function of temperature for catalyst alone (Ni -empty symbols- and NiFe -solid symbols-), MM -star symbols-, and DFM -triangle symbols- synthesized in this study. Experimental conditions: Table 2. Top dashed line: theoretical thermodynamic equilibria.

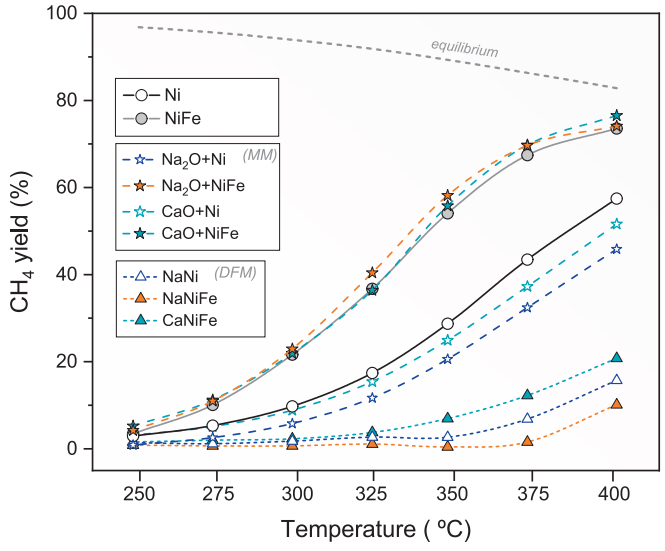

Fig. 6. Conventional methanation. Yield to CH_4 from CO_2 as function of temperature for catalyst alone (Ni and NiFe), MM, and DFM synthesized in this study. Experimental conditions: Table 2.

(2)), described above, have been defined to account for the comparison of the amount of CH_4 produced with a catalyst alone (*NiFe* or *Ni* supported on γ-Al_2O_3) respecting the same catalyst when mixed with *Na_2O* or *CaO* solids (*Mechanical Mixture* -MM-) or when the catalyst is directly impregnated with the equivalent amount of adsorbent Na or Ca (*Dual Function Material* -DFM-).

Among the tested catalysts, the mechanical mixture (MM) of Na_2O/γ-Al_2O_3 with NiFe/ γ-Al_2O_3 (labelled as Na_2O + NiFe) demonstrated the highest methane production rates and the most significant intensification ratio. Additionally, MM system showed no interference between the CO_2 adsorption sites and the catalytic active centers under conventional methanation conditions (Fig. 5 and Fig. 6). Although the DFM configuration may appear more efficient than MM for methane production due to the proximity between active sites for CO_2 adsorption (alkaline/alkaline-earth) and the catalytically active species (Ni or NiFe), empirical results demonstrate that this is not necessarily the case. The reason should be sought in a combination of variables such as reaction conditions, particle size, specific surface area and adsorbent species among others. Similar conclusions were described in a recent work by Porta et al. [35]. Consequently, this MM catalyst was selected for further investigation in the subsequent phase of the study. For catalysts containing calcium (Ca), both methods of adsorbent functionalization resulted in comparable methane production levels.

3.3. Effect of temperature in the adsorption and hydrogenation stages

The adsorption-methanation tests followed a similar scheme to that presented in Fig. 2, where the points represent measurements from the micro-GC, and the continuous lines represent measurements from the gas analyzer (IR). The combination of both instruments allows for more comprehensive data collection. Additionally, the experimental conditions are shown in Table 2 (Adsorption + Methanation cycles).

For the experimental performance tests, two different CO_2 partial pressures in the feed were selected: 40 %^{v} (p_{CO2} = 0.4 bar) and 12 %^{v} (p_{CO2} = 0.12 bar). The selection of these CO_2 concentrations was based on the potential application of the system for direct CO_2 capture from a raw biogas stream—typically containing around 40 %^{v} CO_2—and for simulating the diluted CO_2 content (approximately 12 %^{v}) found in conventional biogas upgrading processes. In order to investigate the influence of CO_2 and assess the feasibility of the hydrogenation step, a temperature range of 200–400 °C was selected.

The results obtained from the temperature study with CO_2 partial pressures of 40 % and 12 % in the feed are presented in Table 4 and Table 5, respectively. The outcomes confirm the feasibility of carrying out the hydrogenation step within the temperature range of 200–400 °C. To this end, the *Methane production* $P^w_{CH_4}[\mu mol/g]$ indicator (Eq. (2) and the *Methanation yield* η_{CH_4}[adim] (Eq. (3) were used.

Table 4 shows at 200 °C, a decrease of more than 50 %^{v} in methane production compared to that at higher temperatures. *Methane production* values ($P^w_{CH_4}$) across three consecutive hydrogenation cycles remained reasonably stable, showing no evidence of catalyst deactivation after 7 h of time-on-stream. Notably, the results at 250 °C demonstrated high methane production under moderate thermal conditions, which are not typically achievable in conventional methanation processes using the same NiFe/γ-Al_2O_3 catalyst, where significantly higher temperatures are required.

The results presented in Table 5 show higher CH_4 yields compared to those in Table 4, indicating that the efficiency of the hydrogenation stage is not only dependent on the amount of CO_2 adsorbed. Furthermore, both experimental sets exhibited similar trends (Fig. 8), with an optimum observed at 350 °C within the studied temperature range. At this temperature, methane production reached its maximum, resulting in significantly elevated yields. Indeed, as shown in Fig. 8, for both experimental series (corresponding to p_{CO2} = 0.4 and p_{CO2} = 0.12), the adsorption capacity of the MM solids mixture decreases with increasing temperature (moving from right to left in the graph). This adsorption capacity ($q^e_{CO_{2,TGA}}[\mu mol/g]$), measured via STA thermogravimetric analysis, is expressed in µmol of adsorbable CO_2 per gram of MM solids. However, while higher temperatures reduce CO_2 adsorption, they simultaneously enhance the methanation of adsorbed CO_2, thereby increasing the process efficiency. This is evidenced by the progressive attainment of higher methanation yields (η_{CH_4}[adim]), as indicated by the dashed *iso*-yield lines. Consequently, methane production ($P^w_{CH_4}[\mu mol/g]$) also increases.

Beyond 350 °C, however, the methanation yields plateau for both series, leading to a net decline in methane production. Although η_{CH_4}[adim] continues to rise marginally at even higher temperatures (400 °C), the diminished adsorption capacity results in an overall reduction in $P^w_{CH_4}[\mu mol/g]$. Thus, the optimal methane production occurs at 350 °C for both CO_2 partial pressures (p_{CO2} = 0.4 and p_{CO2} = 0.12).

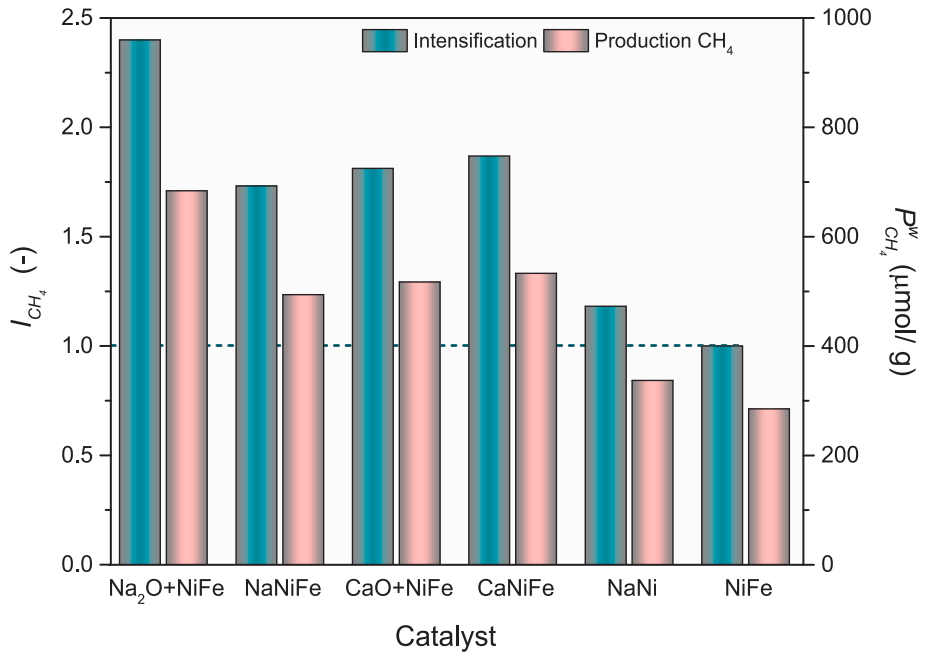

Fig. 7. CO_2 adsorption-methanation cycles. – Intensification I_{CH_4} (Eq. (1)) and Methane production $P^w_{CH_4}$ (Eq. (2)) relative ratios. p_{CO_2} = 0.4 bar, p_{Ar} = 0.6 bar, P_{TOTAL} = 1 bar, Total flow = 150 mL(SATP)/min, Temperature = 400 °C.

Table 4
Methanation cycles with Na_2O + NiFe (MM). Methane production $P^w_{CH_4}$ [μmol/g] and Methanation yield η_{CH_4} [adim] at different temperatures and cycles with 40 %^{v} CO_2 feed. Experimental conditions: Table 2.

Temperature	1st $P^w_{CH_4}$	2nd $P^w_{CH_4}$	3rd $P^w_{CH_4}$	1st η_{CH_4}	2nd η_{CH_4}	3nd η_{CH_4}
400 °C	358	396	399	0.65	0.72	0.73
350 °C	420	467	474	0.60	0.66	0.67
300 °C	437	432	393	0.50	0.49	0.45
250 °C	380	409	401	0.35	0.38	0.37
200 °C	288	212	237	0.22	0.16	0.18

Table 5
Methanation cycles with Na_2O + NiFe (MM). Methane production $P^w_{CH_4}$ [μmol/g] and Methanation yield η_{CH_4} [adim] at different temperatures and cycles with 12 %^{v} CO_2 feed. Experimental conditions: Table 2.

Temperature	1st $P^w_{CH_4}$	2nd $P^w_{CH_4}$	1st η_{CH_4}	2nd η_{CH_4}
400 °C	352	349	0.87	0.86
350 °C	386	389	0.72	0.72
325 °C	393	374	0.66	0.63
300 °C	393	372	0.56	0.53
275 °C	404	360	0.50	0.44
250 °C	323	350	0.36	0.39

3.4. Effect of the purge stage in the adsorption–methanation cycle and the potential use of sweetened biogas as a CO_2 source

To evaluate the effect of introducing a sweetened biogas stream as the CO_2 source during the adsorption step, the partial pressure of CO_2 in the feed was adjusted to 12 %^{v}. This value is representative of conventional methanation processes operating at the stoichiometric H_2:CO_2 molar ratio (4:1), as discussed in previous sections. The biogas composition consisted of a CH_4:CO_2 volumetric ratio of 7:3, further diluted with 5 %^{v} N_2 as an internal standard and Ar as the balance gas.

The introduction of a purge stage between the CO_2 adsorption and hydrogenation steps, yields no significant changes in methane production (Table 6). These findings support the hypothesis that CO_2 capture by Na_2O occurs predominantly via chemisorption, as previously reported by Jeong-Potter et al. [47]. Since the captured CO_2 remains strongly bound to the adsorbent, inert gas purging does not substantially affect the amount of CO_2 available for hydrogenation, thereby leaving methane production unaffected.

In addition, CH_4 production during the methanation stage was not significantly influenced by the presence of CH_4 in the feed during the adsorption step, under the operating conditions tested (Table 6). This observation suggests that CH_4 does not compete with CO_2 for adsorption on Na_2O-based materials. Such behavior supports the potential application of this adsorbent–catalyst system in methane enrichment processes from biogas streams for biogas upgrading.

4. Conclusions

The Mechanical Mixture (MM) of Na_2O/γ-Al_2O_3 with NiFe/γ-Al_2O_3 proved the most effective configuration for methane generation, outperforming integrated Dual Function Materials (DFM) due to the beneficial separation between adsorbent and catalyst phases. Although both Na_2O and CaO were effective adsorbents, Na_2O delivered superior methane yields, attributed to its enhanced CO_2 adsorption and favorable interaction with H_2 in the presence of the NiFe catalyst. MM demonstrated high versatility for both conventional and cyclic methanation, whereas inclusion of the alkali species in DFM negatively affected catalyst structure.

Methane production was strongly influenced by temperature, with optimal yields observed at 250–350 °C. Lowering the reaction temperature to 250 °C offers potential for energy savings, although performance dropped sharply at 200 °C due to insufficient catalytic activity. Higher temperatures led to more efficient CO_2 utilization, likely reflecting decreased adsorption at elevated temperatures.

Experiments at CO_2 partial pressures of 0.12 and 0.40 bar exhibited optimal methane yield at 350 °C. The omission of inert gas purges between cycles did not adversely affect methane output, suggesting process intensification is feasible by using CO_2 (i.e., adsorption stage) for catalyst drying.

The NiFe/γ-Al_2O_3 catalyst combined with Na_2O/γ-Al_2O_3 in the MM configuration exhibited excellent stability and maintained consistent

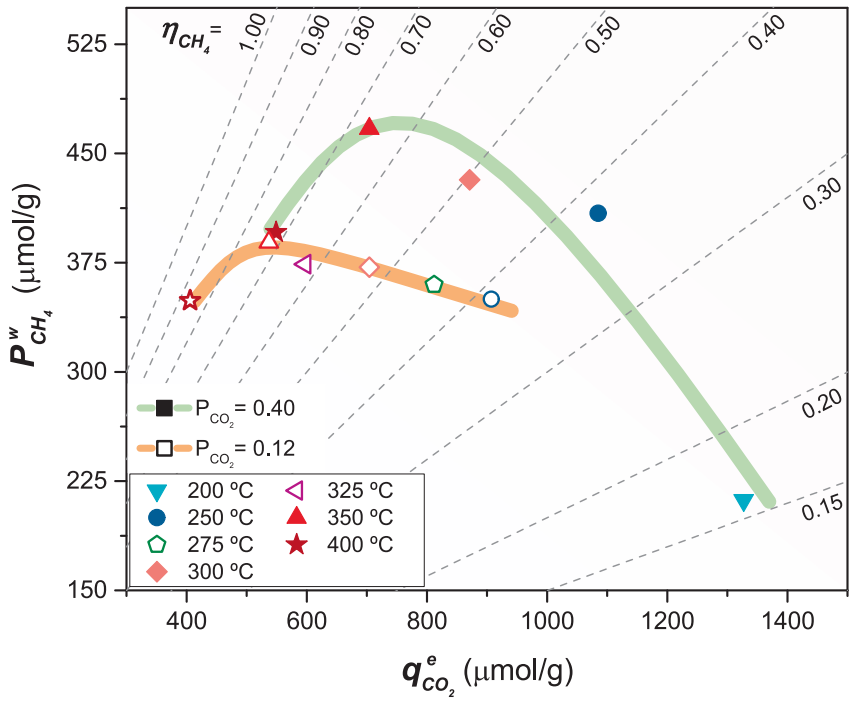

Fig. 8. Methane production $P^{w}_{CH_4}$ [µmol/g_{MM}] versus Adsorption capacity $q^{e}_{CO_{2\cdot TGA}}$ [µmol/g] for two experimental sets conducted at different inlet CO_2 partial pressures: 40 %^{v} (P_{CO2} = 0.40 bar, solid symbols) and 12 %^{v} (P_{CO2} = 0.12 bar, empty symbols). Solid: MM Na_2O + NiFe/Al_2O_3. Data points correspond to different reaction temperatures according to the colors. Dashed lines represent different methanation yields of adsorbed CO_2 η_{CH_4} [adim]. Thick colored lines are for visual guidance only.

Table 6
Methane production $P^{w}_{CH_4}$ [µmol/g_{MM}] and Methanation yield η_{CH_4} [adim] (CH_4 produced per CO_2 adsorbed) over two adsorption–methanation cycles at 400 °C and 350 °C using Na_2O + NiFe. Comparison between conventional cycles and cycles with inert purge or biogas during the adsorption stage. All experiments were conducted with 12 %^{v} CO_2 in the feed; biogas composition includes CH_4: CO_2 = 7:3 M ratio. Experimental conditions as in Table 2.

Experiment sequence	T (°C)	1st $P^{w}_{CH_4}$	2nd $P^{w}_{CH_4}$	1st η_{CH_4}	2nd η_{CH_4}
Cycle CO_2/H_2	400	352	349	0.87	0.86
Cycle CO_2/purge N_2/H_2/ purge N_2	400	341	345	0.84	0.85
Cycle biogas /purge N_2/H_2/ purge N_2	400	344	350	0.85	0.86
Cycle CO_2/H_2	350	386	389	0.72	0.72
Cycle CO_2/purge N_2/H_2/ purge N_2	350	375	400	0.70	0.74
Cycle biogas /purge N_2/H_2	350	380	375	0.71	0.70

methane production over extended cycling (up to 7 h of adsorption-methanation cycles), underscoring its suitability for industrial application.

Experiments incorporating a sweetened biogas-like feed during the adsorption stage showed no detrimental effect on the methane generation process. This result opens promising avenues for utilizing this methodology in biogas upgrading, enabling the production of synthetic natural gas (SNG) compatible with existing natural gas infrastructures.

Credit authorship contribution statement

V.D. Mercader: Writing – original draft, Methodology, Investigation, Formal analysis, Data curation, Conceptualization. **P. Sanz-Monreal:** Writing – original draft, Investigation, Formal analysis, Data curation. **P. Durán:** Supervision, Resources, Methodology. **P. Aragüés-Aldea:** Validation, Investigation, Conceptualization. **E. Francés:** Visualization, Formal analysis, Conceptualization. **J. Herguido:** Writing – review & editing, Visualization, Validation, Supervision, Formal analysis, Conceptualization. **J.A. Peña:** Writing – review & editing, Validation, Supervision, Project administration, Methodology, Funding acquisition, Formal analysis, Conceptualization.

Declaration of competing interest

The authors declare that they have no known competing financial interests or personal relationships that could have appeared to influence the work reported in this paper.

Acknowledgements

This research has been funded by MICIU (Spanish Ministerio de Ciencia, Innovación y Universidades) project number PID2022-136947OB-I00 through the Agencia Estatal de Investigación (AEI) and European Union Next Generation PRTR-C17.I1 Task LA4.A1. Additionally, the consolidated research group Catalysis and Reactor Engineering Group (CREG) (T43-23R) has received financial support from Gobierno de Aragón (Aragón, Spain) through the European Social Fund – FEDER.

In addition, V. D. Mercader (grant no. PRE2020-095679) and P. Aragüés-Aldea express their gratitude for the research predoctoral grants to Spanish Ministerio de Ciencia, Innovación y Universidades (MICIU) and Gobierno de Aragón (Aragón, Spain) respectively.

The authors would like to express their gratitude to the B.Sc. students who conducted their final degree projects on related topics, Beatriz Carreras, Miguel Ángel Becerril, Alejandra Aznar and Jonas Glaser. Their contributions were valuable in establishing the experimental conditions used in this work.

Lastly, authors acknowledge the work of J. Lasobras and Servicio General de Apoyo a la Investigación-SAI (Universidad de Zaragoza).

Data availability

Data will be made available on request.

References

[1] International Energy Agency (IEA). Global Energy Review. 2025.
[2] Hosseini SE. Fossil fuel crisis and global warming. Fundamentals of low emission flameless combustion and its applications. Elsevier 2022:1–11. https://doi.org/10.1016/B978-0-323-85244-9.00001-0.
[3] International Energy Agency (IEA). Renewable Energy Progress Tracker 2024. https://www.iea.org/data-and-statistics/data-tools/renewable-energy-progress-tracker.
[4] Dodds PE, Garvey SD. Energy storage options to balance renewable electricity systems. Storing Energy, Elsevier 2022:13–33. https://doi.org/10.1016/B978-0-12-824510-1.00032-5.
[5] Massol O, Tchung-Ming S, Banal-Estañol A. Capturing industrial CO_2 emissions in Spain: infrastructures, costs and break-even prices. Energy Policy 2018;115:545–60. https://doi.org/10.1016/j.enpol.2018.01.015.
[6] Allah FUM, da Marques A, Carvalho S. Current status, challenges and future prospects of carbon capture and storage (CCS) for thermal power plants in Brazil. Int J Greenhouse Gas Control 2024;136:104198. https://doi.org/10.1016/j.ijggc.2024.104198.
[7] Shen Y, Sun S, Sun H, Xu Y, Zhou H, Wu C, et al. Dual functional materials for integrated CO_2 capture and utilization (ICCU): design, fabrication, performances, and challenges. Chem Eng J 2025;512:162440. https://doi.org/10.1016/j.cej.2025.162440.
[8] Sarmad S, Lu D, Gao S, Sun Z, Zhou Z, Ali A, et al. Advancing syngas production: a comparative techno-economic analysis of ICCU and CCU technologies for CO_2 emission reduction. J Environ Chem Eng 2024;12:114562. https://doi.org/10.1016/j.jece.2024.114562.
[9] Sabatier P, Senderens J. Nouvelles synthèses du méthane. C R Acad Sci Paris 1902:514–6.
[10] Sanz-Monreal P, Mercader VD, Aragüés-Aldea P, Durán P, Francés E, Herguido J, et al. Techno-economic assessment of a plant for the upgrading of MSW biogas to synthetic natural gas by thermocatalytic methanation. Biomass Bioenergy 2025;198:107871. https://doi.org/10.1016/j.biombioe.2025.107871.
[11] Tommasi M, Degerli SN, Ramis G, Rossetti I. Advancements in CO_2 methanation: a comprehensive review of catalysis, reactor design and process optimization. Chem Eng Res Des 2024;201:457–82. https://doi.org/10.1016/j.cherd.2023.11.060.
[12] Duyar MS, Treviño MAA, Farrauto RJ. Dual function materials for CO_2 capture and conversion using renewable H_2. Appl Catal B 2015;168–169:370–6. https://doi.org/10.1016/j.apcatb.2014.12.025.
[13] Jeong-Potter C, Zangiabadi A, Farrauto R. Extended aging of Ru-Ni, Na_2O/Al_2O_3 dual function materials (DFM) for combined capture and subsequent catalytic methanation of CO_2 from power plant flue gas. Fuel 2022;328. https://doi.org/10.1016/j.fuel.2022.125283.
[14] Jeong-Potter C, Abdallah M, Kota S, Farrauto R. Enhancing the CO_2 adsorption capacity of γ-Al_2O_3 supported alkali and alkaline-earth metals: impacts of dual function material (DFM) preparation methods. Ind Eng Chem Res 2022;61:10474–82. https://doi.org/10.1021/acs.iecr.2c00364.
[15] Sun H, Sun S, Liu T, Zeng J, Wang Y, Yan Z, et al. Integrated CO_2 Capture and utilization: selection, matching, and interactions between adsorption and catalytic sites. ACS Catal 2024;14:15572–89. https://doi.org/10.1021/acscatal.4c03861.
[16] Tsiotsias AI, Charisiou ND, Yentekakis IV, Goula MA. The role of alkali and alkaline earth metals in the CO_2 methanation reaction and the combined capture and methanation of CO_2. Catalysts 2020;10:812. https://doi.org/10.3390/catal10070812.
[17] Martins JA, Miguel CV, Rodrigues AE, Madeira LM. Novel adsorption–reaction process for biomethane purification/production and renewable energy storage. ACS Sustain Chem Eng 2022;10:7833–51. https://doi.org/10.1021/acssuschemeng.1c06844.
[18] Faria C, Rocha C, Miguel C, Rodrigues A, Madeira LM. Process intensification concepts for CO_2 methanation – a review. Fuel 2025;386:134269. https://doi.org/10.1016/j.fuel.2024.134269.
[19] Pandey D, Ray K, Bhardwaj R, Bojja S, Chary KVR, Deo G. Promotion of unsupported nickel catalyst using iron for CO_2 methanation. Int J Hydrogen Energy 2018;43:4987–5000. https://doi.org/10.1016/j.ijhydene.2018.01.144.
[20] Jeong-Potter C, Zangiabadi A, Farrauto R. Extended aging of Ru-Ni, Na_2O/Al_2O_3 dual function materials (DFM) for combined capture and subsequent catalytic methanation of CO_2 from power plant flue gas. Fuel 2022;328:125283. https://doi.org/10.1016/j.fuel.2022.125283.
[21] Zhou J, Dang C, Zheng G, Cai W. The capture and in-situ hydrogenation of CO_2 over Ni-CaO-$Ca_{12}Al_{14}O_{33}$ bifunctional catalyst. Sep Purif Technol 2025;354:129375. https://doi.org/10.1016/J.SEPPUR.2024.129375.
[22] Zhou J, Zhang W, Cai W, Dang C. High stability for the integrated CO_2 capture and methanation reaction over the MgO-modified Ni-CaO bifunctional catalyst. Sep Purif Technol 2025;366:132845. https://doi.org/10.1016/J.SEPPUR.2025.132845.
[23] Medina OE, Amell AA, López D, Santamaría A. Comprehensive review of nickel-based catalysts advancements for CO_2 methanation. Renew Sustain Energy Rev 2025;207:114926. https://doi.org/10.1016/j.rser.2024.114926.
[24] Zhang L, Li Z, Gao Y, Li Q, Deng Z, Miao B, et al. Recent advances in supported metal catalysts for CO_2 methanation: mechanisms, materials design, and the promise of perovskite-based supports. Energy Convers Manage: X 2025;27:101066. https://doi.org/10.1016/j.ecmx.2025.101066.
[25] Rönsch S, Schneider J, Matthischke S, Schlüter M, Götz M, Lefebvre J, et al. Review on methanation – from fundamentals to current projects. Fuel 2016;166:276–96. https://doi.org/10.1016/j.fuel.2015.10.111.
[26] Costmine Intelligence. Mining Cost Service n.d. https://www.costmine.com/.
[27] Su X, Shen L. Advances and challenges about Ni-based dual functional materials for alternating cycles of CO_2 storage and in-situ hydrogenation to CH_4. Carbon Capture Sci Technol 2024;13:100278. https://doi.org/10.1016/j.ccst.2024.100278.
[28] Spennati E, Riani P, Garbarino G. A perspective of lanthanide promoted Ni-catalysts for CO_2 hydrogenation to methane: catalytic activity and open challenges. Catal Today 2023;418:114131. https://doi.org/10.1016/j.cattod.2023.114131.
[29] Bermejo-López A, Pereda-Ayo B, González-Marcos JA, González-Velasco JR. Mechanism of the CO_2 storage and in situ hydrogenation to CH_4. Temperature and adsorbent loading effects over Ru-CaO/Al_2O_3 and Ru-Na_2CO_3/Al_2O_3 catalysts. Appl Catal B 2019;256. https://doi.org/10.1016/j.apcatb.2019.117845.
[30] Bermejo-López A, Pereda-Ayo B, González-Marcos JA, González-Velasco JR. Ni loading effects on dual function materials for capture and in-situ conversion of CO_2 to CH_4 using CaO or Na_2CO_3. J CO2 Util 2019;34:576–87. https://doi.org/10.1016/j.jcou.2019.08.011.
[31] Tsiotsias AI, Charisiou ND, Yentekakis IV, Goula MA. Bimetallic Ni-based catalysts for CO_2 methanation: a review. Nanomaterials 2021;11:1–34. https://doi.org/10.3390/nano11010028.
[32] Bermejo-López A, Pereda-Ayo B, González-Marcos JA, González-Velasco JR. Alternate cycles of CO_2 storage and in situ hydrogenation to CH_4 on Ni-Na_2CO_3/Al_2O_3: influence of promoter addition and calcination temperature. Sustain Energy Fuels 2021;5:1194–210. https://doi.org/10.1039/d0se01677b.
[33] Sanz-Martínez A, Durán P, Mercader VD, Francés E, Peña JÁ, Herguido J. Biogas upgrading by CO_2 methanation with Ni-, Ni–Fe-, and Ru-based catalysts. Catalysts 2022;12:1609. https://doi.org/10.3390/catal12121609.
[34] Chai KH, Leong LK, Sethupathi S, Lim S, Pang YL, Yap YH. Overcoming oxidation-induced deactivation of Ni-based dual-function materials in integrated sequential carbon capture and methanation with Ni/CeO_2 catalyst and "Na_2O"/Al_2O_3 sorbent in adjacent beds. Int J Hydrogen Energy 2025;103:23–33. https://doi.org/10.1016/j.ijhydene.2025.01.188.
[35] Porta A, Coffano C, Piacentini M, Rabino F, Picutti B, Lietti L, et al. One-pot CO2-to-olefins via methanol over In2O3-ZrO2/SAPO-34 catalysts mixtures with different spatial arrangements. Appl Catal A 2024;682:119799. https://doi.org/10.1016/J.APCATA.2024.119799.
[36] Guo ZK, Gao S, Xiang SX, Wang JP, Mao GC, Jiang HL, et al. Mechanochemical synthesis of Ni/MgO dual functional materials at room temperature for CO_2 capture and methanation. Chem Eng J 2024;481:148599. https://doi.org/10.1016/J.CEJ.2024.148599.
[37] Mercader VD, Durán P, Aragüés-Aldea P, Francés E, Herguido J, Peña JA. Biogas upgrading by intensified methanation (SESaR): reaction plus water adsorption - desorption cycles with Ni-Fe/Al_2O_3 catalyst and LTA 5A zeolite. Catal Today 2024;433:114667. https://doi.org/10.1016/j.cattod.2024.114667.
[38] Cañada-Barcala A, Larriba M, Águeda Maté VI, Delgado Dobladez JA. Synthetic natural gas production through biogas methanation using a sorption-enhanced reaction process. Sep Purif Technol 2024;331:125714. https://doi.org/10.1016/j.seppur.2023.125714.
[39] Wei L, Azad H, Haije W, Grenman H, de Jong W. Pure methane from CO_2 hydrogenation using a sorption enhanced process with catalyst/zeolite bifunctional materials. Appl Catal B 2021;297:120399. https://doi.org/10.1016/j.apcatb.2021.120399.
[40] Gómez L, Martínez I, Navarro MV, Murillo R. Selection and optimisation of a zeolite/catalyst mixture for sorption-enhanced CO_2 methanation (SEM) process. J CO2 Util 2023;77:102611. https://doi.org/10.1016/j.jcou.2023.102611.
[41] Mercader VD, Aragüés-Aldea P, Durán P, Francés E, Herguido J, Peña JA. Optimizing Sorption Enhanced Methanation (SEM) of CO_2 with Ni_3Fe + LTA 5 A mixtures. Catal Today 2025;453:115262. https://doi.org/10.1016/j.cattod.2025.115262.
[42] Chen J, Xu Y, Liao P, Wang H, Zhou H. Recent progress in integrated CO_2 capture and conversion process using dual function materials: a state-of-the-art review. Carbon Capture Sci Technol 2022;4:100052. https://doi.org/10.1016/j.ccst.2022.100052.
[43] Marin J, Parra P, Rios L. Improved dual function materials for CO_2 capture and in situ methanation. Energ Technol 2024;12. https://doi.org/10.1002/ente.202300952.
[44] Liu K, Xu X, Xu J, Fang X, Liu L, Wang X. The distributions of alkaline earth metal oxides and their promotional effects on Ni/CeO_2 for CO_2 methanation. J CO2 Util 2020;38:113–24. https://doi.org/10.1016/j.jcou.2020.01.016.
[45] Mohammed AAA, Ebrahimi P, Yuda A, Al-Marri MJ, Kumar A, Ali M, et al. Role of Ca in Ni-Ca/fumed-SiO_2 catalysts for CO_2 catalytic conversion to methane. Top Catal 2024. https://doi.org/10.1007/s11244-024-02010-x.
[46] Zheng Q, Farrauto R, Chau NA. Adsorption and methanation of flue gas CO_2 with dual functional catalytic materials: a parametric study. Ind Eng Chem Res 2016;55:6768–76. https://doi.org/10.1021/acs.iecr.6b01275.
[47] Jeong-Potter C, Abdallah M, Sanderson C, Goldman M, Gupta R, Farrauto R. Dual function materials (Ru+Na_2O/Al_2O_3) for direct air capture of CO_2 and in situ catalytic methanation: the impact of realistic ambient conditions. Appl Catal B 2022;307:120990. https://doi.org/10.1016/j.apcatb.2021.120990.
[48] Duyar MS, Wang S, Arellano-Treviño MA, Farrauto RJ. CO_2 utilization with a novel dual function material (DFM) for capture and catalytic conversion to synthetic natural gas: an update. J CO2 Util 2016;15:65–71. https://doi.org/10.1016/j.jcou.2016.05.003.

[49] Fan L, Chen L, Liu D, Sun L, Qin C. Synthetic natural gas production via pressurized integrated carbon capture and in-situ methanation of Ni-Na_2CO_3/γ-Al_2O_3 dual function material. Energy Convers Manag 2025:326. https://doi.org/10.1016/j.enconman.2025.119510.

[50] Kumar Prabhakar J, Apte PA, Deo G. Exploring optimal total metal loading of Ni_3Fe/Al_2O_3 catalyst for CO_2 methanation and its kinetic model. Fuel 2024;367. https://doi.org/10.1016/j.fuel.2024.131447.

[51] Cimino S, Boccia F, Lisi L. Effect of alkali promoters (Li, Na, K) on the performance of Ru/Al_2O_3 catalysts for CO_2 capture and hydrogenation to methane. J CO2 Util 2020;37:195–203. https://doi.org/10.1016/j.jcou.2019.12.010.

[52] Chapter 12 Decomposition of carbonates, studies in physical and theoretical chemistry 86 (1999) 345–364. https://doi.org/10.1016/S0167-6881(99)80014-7.